5-25-2013

Performance of Solid Oxide Iron-Air Battery Operated at 550°C

Xuan Zhao
University of South Carolina - Columbia, zhao53@email.sc.edu

Yunhui Gong

Xue Li
University of South Carolina - Columbia, lixue@cec.sc.edu

Nansheng Xu
University of South Carolina - Columbia, xun@cec.sc.edu

Kevin Huang
University of South Carolina - Columbia, huang46@cec.sc.edu

Publication Info

Published in *Journal of The Electrochemical Society*, Volume 160, Issue 8, 2013, pages A1241-A1247.

Publisher's Version: http://dx.doi.orgg/10.1149/2.085308jes
Zhao, X., Gong, Y., Li, X., Xu, N., & Huang, K. (2013). Performance of Solid Oxide Iron-Air Battery Operated at 550°C. Journal of The Electrochemical Soceity, 160 (8), A1241 - A1247. http://dx.doi.org/10.1149/2.085308jes

0013-4651/2013/160(8)/A1241/7/$31.00 © The Electrochemical Society

Performance of Solid Oxide Iron-Air Battery Operated at 550°C

Xuan Zhao,* Yunhui Gong, Xue Li, Nansheng Xu, and Kevin Huang,z**

Department of Mechanical Engineering, University of South Carolina, Columbia, South Carolina 29201, USA

"Metal-air" batteries have garnered much attention in recent years due to their high intrinsic specific energy and use of inexhaustible and storage-free oxygen source -air- for the "metal-oxygen" reaction. In this study, we report the performance of a new type of all solid-state "iron-air" battery operated at 550°C. The results show that CeO_2 nanoparticles incorporated into the Fe-Fe_3O_4 redox-couple can improve the specific energy (Wh/kg) and round trip efficiency by 15% and 29%, respectively, over the baseline Fe-Fe_3O_4 battery. Use of supported Fe-Fe_3O_4 nanoparticles as the redox couple can increase the specific energy and round-trip efficiency by 13% and 48% over the baseline battery, respectively. However, the nanoparticle redox-couple is susceptible to thermal coarsening under operating conditions, causing cycle stability problem. Future research needs to focus on improving battery's performance and stability by utilizing thin-film electrolyte and high-performance and stable electrodes, and preventing thermal growth of active redox couple nanoparticles. A most recent testing on an optimized battery component has shown promising results: discharge specific energy can reach 91.0% of the maximum theoretical specific energy with a round-trip efficiency of 82.5%.
 [DOI: 10.1149/2.085308jes]

Manuscript submitted April 10, 2013; revised manuscript received May 3, 2013. Published May 25, 2013.

The "Metal-air" batteries have the potential to offer high specific energy without the need to store oxygen for the "metal-oxygen" chemistry. The modern "metal-air" batteries, either primary or secondary, have primarily employed two types of ionic conductors as the electrolyte: cation conductors (e.g., Li^+-conductor for "Li-air") or anion conductors (e.g., alkaline OH^--conductor for "Zn-air" and "Fe-air").[1–4] Despite exhibiting high initial specific energy, these batteries typically suffer from fast decay in performance upon cycling, resulting in very poor round-trip efficiency and short cycle-life. Evidence gathered from in-situ spectroscopic and microscopic studies explicitly reveals air-electrode and electrolyte as the primary sources of performance degradation: congestion of air-pathway by the formation of condensed oxides,[5] precipitation of carbonate in the air-electrode electro-catalyst's pores,[6,7] and evaporation/decomposition of liquid electrolytes.[6,7–10]

Recently, we demonstrated a new type of high-temperature "metal-air" battery based on reversible solid oxide fuel cell (RSOFC) and redox-couple energy storage unit.[11–15] The RSOFC consists of a perovskite-structured oxide air-electrode, a solid oxide-ion electrolyte and a Ni-based fuel-electrode. The redox-couple energy storage unit is comprised of a pair of metal/metal-oxide. The dual functionality of a RSOFC, i.e. fuel-cell and electrolyzer modes, is utilized in the new "metal-air" battery as the means of discharging and charging, respectively, while the chemical energy are simultaneously stored in the metal/metal-oxide redox couple through a H_2/H_2O mediated redox reaction. During operation, the air-electrode reactions involve only reduction and evolution of gaseous O_2, making air-pathway clogging no longer an issue. In addition, solid oxide-ion electrolytes are known to be stable in a broad range of gas mixtures and in contact with a variety of oxides.[16–18] Therefore, this new all solid-state "metal-air" battery is free of the problems faced by the conventional liquid-electrolyte based "metal-air" batteries. Furthermore, by inheriting all the merits of the solid oxide fuel cell technology, it is well-suited for large-scale stationary grid energy storage.

While the high operating temperature is an advantage to promote high conductivity in the electrolyte and fast reaction kinetics in electrodes and redox-couple, it does present challenges to the durability and cost of the battery. Therefore, an optimal temperature window that can best balance kinetics, durability and cost is needed. For the development of RSOFC, a well-accepted temperature window is within 550–650°C where reasonably fast kinetics can be maintained with improved durability and reduced cost.

Selection of the same operating temperature window for the solid oxide "metal-air" battery (SOMAB) is also beneficial to the energy storage. As the temperature decreases, the maximum theoretical specific energy (MTSE) becomes higher, and more importantly the coarsening of fine metal-particles in the redox-couple can be mitigated, thus extending the lifetime of a SOMAB. Fig. 1 shows the comparison of MTSE and EMF of Fe-FeO and Fe-Fe_3O_4 redox couples, two suitable energy storage materials for the solid oxide "iron-air" battery. According to the Fe-O phase diagram, the former is thermodynamically stable at $t > 600°C$, whereas the latter is only stable at $t \leq 600°C$. It is evident from Fig. 1 that the Fe-Fe_3O_4 stable at $t \leq 600°C$ possesses a higher EMF and MTSE than those of Fe-FeO stable at $t > 600°C$. A much higher discharge capacity (>1,000 mAh/g) has indeed been experimentally observed on Fe-Fe_3O_4 as the redox-couple at 600°C,[19,20] although it was H_2 not electricity used to recharge the battery.

A key to the success of such an intermediate-temperature (IT) SOMAB is to retain the kinetic performance of both RSOFC and redox-couple in the battery. While there has been significant progress made in recent years in the area of IT-RSOFC, which can be beneficial to the development of the IT-SOMAB, information on the kinetics of H_2-H_2O mediated metal/metal-oxide redox reaction is rather scarce in the literature.

In this study, we report that the performance of IT-SOMAB operated at 550°C can be enhanced by either applying redox-active catalyst or increasing the surface area of active redox-couple particles in the energy storage unit. From the obtained results, the effects of catalysts and reactive surface areas on the redox kinetics of Fe-Fe_3O_4 are discussed.

Experimental

Synthesis of Fe-Fe_3O_4 redox couple.— The baseline Fe-Fe_3O_4 redox couple in the IT-SOMAB was derived from a precursor synthesized by a chemical co-precipitation method. An aqueous solution containing 0.1 M $Fe(NO_3)_3 \cdot 9H_2O$ (Alfa Aesar, 98.0–101.0%) and $ZrO(NO_3)_2 \cdot 4H_2O$ (Alfa Aesar, 99.9%) was peptized by $(NH_4)_2CO_3$, precipitating out Fe and Zr hydroxides simultaneously. The use of ZrO_2 is intended to mitigate the coarsening of Fe-particles during operation. The atomic ratio of Fe:Zr in the starting aqueous solutions was prepared in such a way that the Fe:Zr ratio in the final mixture was at 42.5:15. To ensure a full precipitation of all the cations in the solution, the molar ratio of $(NH_4)_2CO_3$ and M^{n+} (M = Zr and Fe) was kept as $n_{(NH_4)_2CO_3} : n_{M^{n+}} = 2.5 : 1$. The precipitates were then filtered, washed, dried and finally calcined at 600°C for 2 h. The formation of the desirable oxides Fe_2O_3 and ZrO_2 was confirmed by X-ray diffraction with no impurity phase. The prepared powders were then mixed with a pore former, pressed into small granules and finally sintered in air at 1000°C for 1 hour. Thus fabricated granules possess an averaged porosity of 70% and a BET surface area of ~3 m^2/g.

To study the effect of catalyst on the redox kinetics of Fe-Fe_3O_4, CeO_2 nanoparticles were dispersed into the aforementioned Fe_2O_3/ZrO_2 granules by solution infiltration technique. To be

*Electrochemical Society Student Member.
**Electrochemical Society Active Member.
zE-mail: kevin.huang@sc.edu

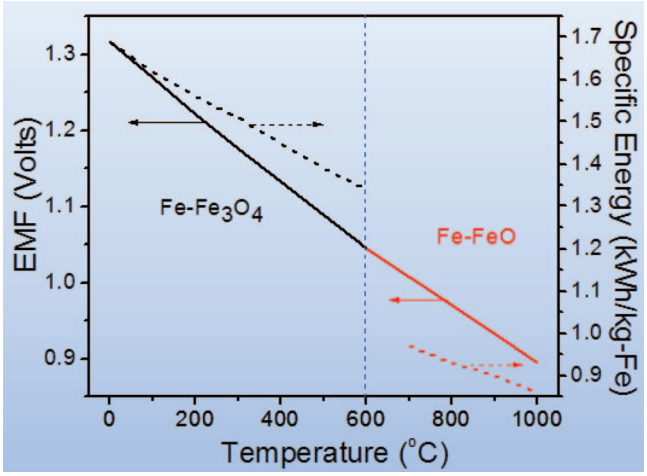

Figure 1. Plots of Nernst potential (EMF) and specific energy of solid oxide "iron-air" battery as a function of temperature. Solid lines: EMF; dashed lines: specific energy.

specific, a 2.0 M aqueous solution of $Ce(NO_3)_3 \cdot 6H_2O$ mixed with a dispersant Triton-X100 (3 wt%) was impregnated into the porous Fe_2O_3/ZrO_2 under a vacuum condition for 8 times. For each impregnation, there was a 100°C-drying and 500°C-calcination step. The final CeO_2 nanoparticles dispersed Fe_2O_3/ZrO_2 was obtained by firing the mixture at 600°C in air for 1 h. The final weight pickup was estimated around 4.5%.

The effect of surface area of active metals on the redox kinetics was also investigated. To acquire fine particles of Fe, an aqueous solution of $Fe(NO_3)_3$ was infiltrated into a commercial porous ZrO_2 catalyst support (Alfa Aesar, surface area: 51 g/m^2) using a modified one-step infiltration procedure.[21,22] Specifically, a 2 M $Fe(NO_3)_3$ aqueous solution was first mixed with Triton-X100 (3 wt%) in DI water, into which the porous ZrO_2 pellets were immersed. During the soaking, the solution was gradually heated to 80°C while the air trapped in the porous ZrO_2 pellets was driven out of the solution, allowing the maximum loading of Fe into the pores of ZrO_2. When no bubbles were visible and the solution finally became viscous, the ZrO_2 pellets filled with $Fe(NO_3)_3$ were then removed, followed by drying at RT and finally calcining at 600°C for 2 h. The final weight gain in term of Fe was estimated to be 10%.

Battery assembly.— A simple planar button cell configuration was employed for all the battery tests in this study, schematic of which

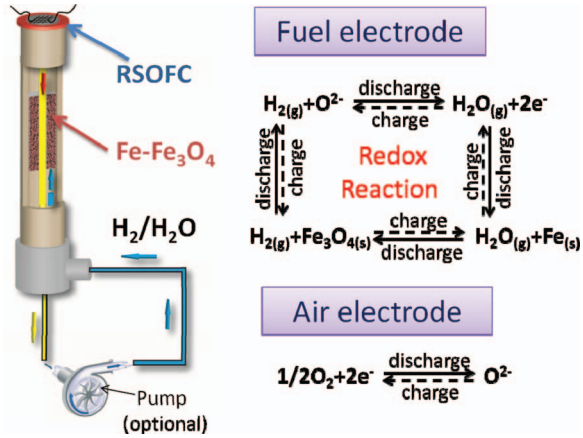

Figure 2. A planar button cell configuration for testing rechargeable solid oxide "iron-air" battery.

Table I. Materials employed in RSOFC of the IT-SOMAB.

Component	Composition	Thickness (μm)
Anode	LDC($Ce_{0.6}La_{0.4}O_{2-\delta}$) -Ni/GDC($Ce_{0.8}Gd_{0.2}O_{2-\delta}$)-Ni	50
Electrolyte	LSGM ($La_{0.8}Sr_{0.2}Ga_{0.83}Mg_{0.2}O_{3-\delta}$)[23]	350
Cathode	LSCF ($La_{0.6}Sr_{0.4}Co_{0.2}Fe_{0.8}O_{3-\delta}$)	50
Current collector	Silver/silver mesh	10

is shown in Fig. 2. The RSOFC consisted of a Sr-and Mg-doped $LaGaO_3$ (LSGM) electrolyte,[23] Sr-and Co-doped $LaFeO_3$ (LSCF) air-electrode and Ni-CeO_2 based fuel electrode, all homemade in our lab. The active cell area was 1.30 cm^2. Table I summarizes the composition and thickness of the functional components in the RSOFC. The active redox couple material Fe-Fe_3O_4 was situated below the surface of fuel-electrode (not in contact). The active Fe loading was controlled within 0.6–0.7 grams for each test. Not shown in Fig. 2 is the homemade glass used to seal the battery. For more experimental details, readers can refer to our previous publications.[11–15]

Battery characterization.— At the beginning of a test, the Fe_2O_3-ZrO_2 granules were first exposed to a mixture of 5%H_2-N_2 during heating. Once reached the melting temperature of the sealing glass around 650°C, a pure H_2 was then introduced to fully reduce Fe_2O_3 into metallic Fe. After approximately a half-hour holding to allow the glass to settle, the temperature was then gradually ramped down to the testing temperature of 550°C. The Fe-Fe_3O_4 redox couple was created in-situ by applying a small discharge current from the RSOFC. To ensure the attainment of Fe-Fe_3O_4 redox couple without over-oxidizing the Fe, the EMF of the RSOFC was closely monitored during the electrochemical oxidation by intermittently switching between the discharging and OCV states. As soon as the EMF reached 1.067 volts, the theoretical Nernst potential for the Fe-Fe_3O_4 equilibrium, the electrochemical oxidation was stopped, and the system was ready for the charge-discharge cycles. During the cycles, the reaction gas H_2-H_2O was also circulated in a closed-loop to homogenize the concentration of the reactants. To prevent water condensation, all pipelines were heat-wrapped and kept at 110°C.

A Solartron 1260/1287 Electrochemical System was employed to characterize the electrical performance of the battery with software modules such as OCV-t, impedance spectroscopy, potential-dynamics, galvanic-dynamics and galvanic cycles.

The microstructures of RSOFC and redox couple, either pre-tested or post-tested, were examined with a field-emission scanning electron microscopy (FESEM, Zeiss Ultra) equipped with an energy dispersive X-ray spectroscopy (EDS) analyzer. The post-tested samples contained a majority of Fe mixed with ZrO_2 as a result of being cooled down in 5%H_2-N_2 protective gas.

Results and Discussion

The performance of the baseline battery.— The baseline battery contains the pellets of Fe-Fe_3O_4 redox-couple prepared from the co-precipitation method described above. Fig. 3 shows the cycling performance characterized under the conditions of t = 550°C, J = 10 mA/cm^2 and n = 10 continuous 2-h discharge and 2-h charge cycles. The current density necessary to achieve a meaningful cell voltage was largely limited by the performance of the RSOFC operated at this low temperature.

The discharge specific energy (DSE) was calculated from the amount of Fe consumed by the oxygen flux (or current density) from the RSOFC, averaging 892 Wh/kg · Fe. Similarly, the charge specific energy (CSE) was averaged to be 2,203 Wh/kg · Fe, yielding a round-trip efficiency of 40.5%. It should be noted that the normalization of the specific energy to the amount of Fe consumed by the oxygen flux allows for a direct comparison with the MTSE, difference of which reveals the scale of the battery's inefficiency. The

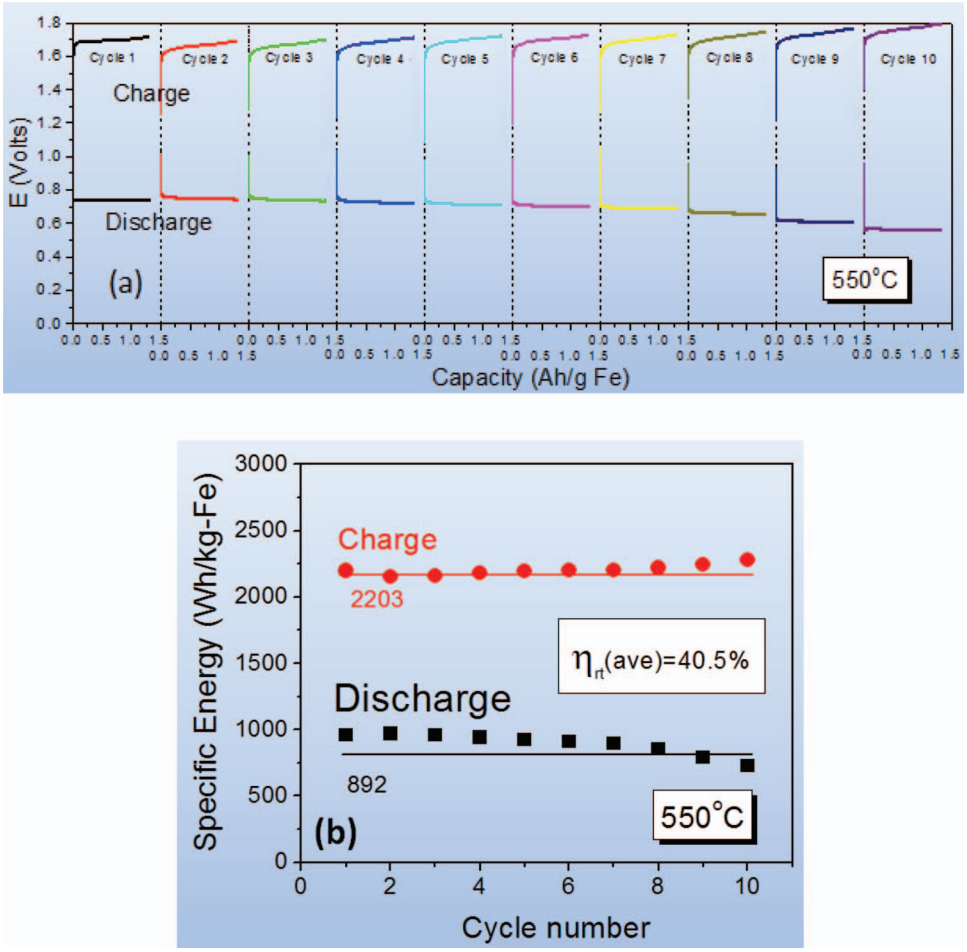

Figure 3. The performance of the baseline battery operated at 550°C for 10 continuous cycles with single-cycle duration of 2 hours under a current density of 10 mA/cm^2; (a) E vs charge capacity; (b) averaged specific energy vs number of cycles.

obtained DSE is evidently lower than the MTSE = 1,360 Wh/kg · Fe calculated from $\Delta G_r°(550°C)$ of the iron-oxygen reaction $3Fe + 2O_2 = Fe_3O_4$. This difference (DSE amounts to 65.6% of MTSE) reflects the degree of energy loss to the electrical polarizations of RSOFC and kinetic resistance of Fe/Fe_3O_4 redox couple. Indeed, the RSOFC for the test employed a thick LSGM electrolyte membrane (350 μm, see Table I) and electrode materials that have not been fully optimized for operating at 550°C. With the use of electrode-supported thin-film electrolytes and more active electrode (particularly air-electrode) materials, the energy loss is expected to be lesser and efficiency to be higher.

The low round-trip efficiency is another sign of energy loss and irreversible redox kinetics. It is known that the total cell resistance of a RSOFC operating under "electrolysis" mode has a tendency to be greater than that of "fuel-cell" mode, which can result in a reduced round-trip efficiency. On the other hand, the lower kinetic rate of Fe_3O_4-reduction to Fe than the oxidation of Fe to Fe_3O_4 also decreases the round-trip efficiency. Overall, the 550°C Fe/Fe_3O_4 battery has ample rooms to further improve its specific energy and efficiencies by optimizing the components of RSOFC (e.g., use of new cell materials and optimization of microstructure) and promoting the redox kinetics (e.g., use of catalysts, use of fine-particle active metals).

Performance of the battery with CeO_2-added Fe-Fe_3O_4 redox couple.— As a means of promoting the redox kinetics, nanoparticles of CeO_2 were incorporated into the microstructure of Fe-Fe_3O_4 as a catalyst, testing result of which is shown in Fig. 4. The battery was cycled for 10 times under the conditions of t = 550°C, J = 10 mA/cm^2 and cycle duration of 2 hours. Compared to Fig. 3 of the baseline battery, the improvement is evident in discharging cycle: higher and more stable voltage. The DSE reached 1,026 Wh/kg · Fe, yielding a round-trip efficiency of 52.2% when compared to the CSE = 1,971 Wh/kg · Fe. These results represent a 15% and 29% improvement in specific energy and round-trip efficiency, respectively, over the baseline battery. It also appears that there was no apparent performance decay over the 10 continuous repeated charge-discharge cycles.

The promotion of redox reaction kinetics by CeO_2 has been well documented in the literature.[24–27] The mixed valence of Ce^{4+}/Ce^{3+} in low partial pressures of oxygen contributes additional catalytic activity to the primary Fe-Fe_3O_4 redox reaction. Previous studies have also reported that Ce can retain the redox activity of Fe-oxides for repeated redox cycles.[24] On the other hand, nanoparticle catalysts can boost the rate of redox reaction by increased reactive area. Fig. 5 shows the morphologies of CeO_2 nanoparticles before and after tests. The original particle sizes of CeO_2 particles were ~50 nm, and increased to approximately 60 nm after testing. Although the finely dispersed CeO_2 nanoparticles appear to have been sintered, the adherence of CeO_2 to the Fe/ZrO_2 backbones seems to have little effect on the catalytic activity of CeO_2 as suggested in Fig. 3.

Performance of the battery with nanoparticle Fe-Fe_3O_4 redox couple.— The active metal Fe in the form of nanoparticles supported on porous ZrO_2 substrate was also evaluated as the energy storage medium, result of which is shown in Fig. 6. The battery was operated at the same condition as the CeO_2-catalyzed battery of Fig. 4. Compared to Fig. 3 of the baseline battery, the improvement is also notable.

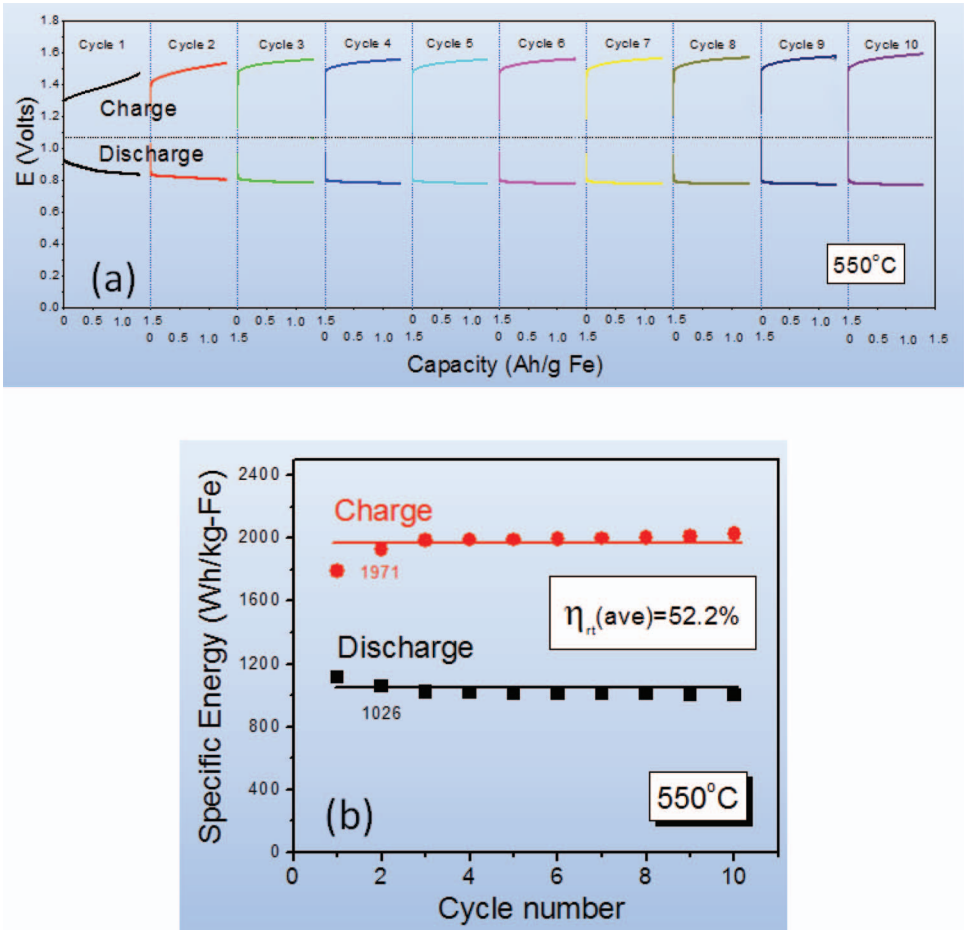

Figure 4. The performance of the CeO_2-catalyzed battery operated at 550°C for 10 continuous cycles with single-cycle duration of 2 hours under a current density of 10 mA/cm^2; (a) E vs charge capacity; (b) averaged specific energy vs number of cycles.

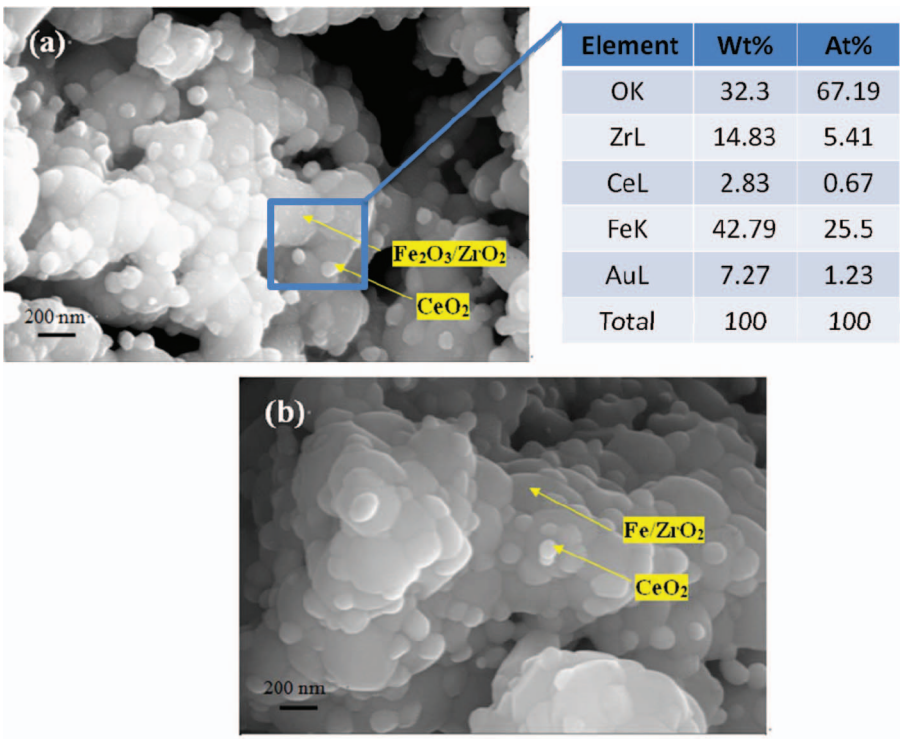

Element	Wt%	At%
OK	32.3	67.19
ZrL	14.83	5.41
CeL	2.83	0.67
FeK	42.79	25.5
AuL	7.27	1.23
Total	100	100

Figure 5. SEM images of CeO_2 nanoparticles inside Fe-based energy storage unit before (a) and after (b) tests.

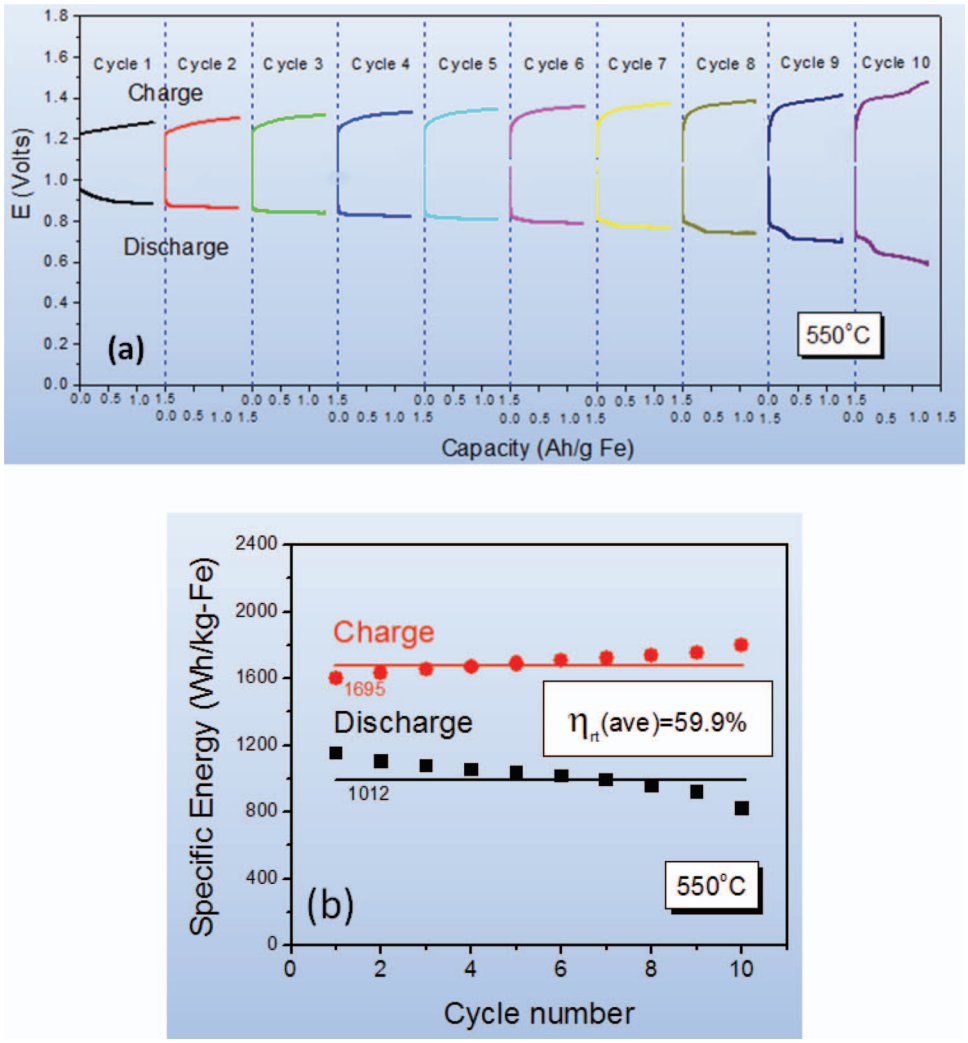

Figure 6. The performance of the battery with nanoparticle active Fe supported on porous ZrO_2 operated at 550°C for 10 continuous cycles with single-cycle duration of 2 hours under a current density of 10 mA/cm^2; (a) E vs charge capacity; (b) averaged specific energy vs number of cycles.

The DSE reached 1,012 Wh/kg · Fe, yielding a round-trip efficiency of 59.9% with CSE = 1,695 Wh/kg · Fe. These results represent 13% and 48% improvement in specific energy and round-trip efficiency, respectively, over the baseline battery. When compared to Fig. 4 of the CeO_2-catalyzed battery, the major improvement is the lowered charging voltage, which is also the reason for the higher round-trip efficiency.

The issue of the nanoparticle redox couple is the poor cycle stability. This is likely caused by the thermal coarsening of these nanoparticles, resulting in a gradual loss of reactive surface area. The morphological change of the Fe nanoparticles in Fig. 7 seems to support this assertion by showing the flaking morphology of Fe_2O_3 precursor before the test and a cluster of sintered Fe-grains after the test.

A general discussion on the sources of performance degradation.— Besides thermal coarsening of the active metal particles during operation, another source of battery performance degradation arises from the RSOFC itself. Fig. 8 shows an example of AC impedance spectra of the baseline battery before and after cycling at 550°C. It is evident that the polarization area-specific-resistance (ASR) of the cell increased significantly after the test. In our previous study,[12] it has been shown that "vapor transport and condensation" phenomenon could be a mechanism leading to an increase in fuel-electrode ASR. Therefore, developing a stable fuel-electrode for RSOFC is equally important in the future research.

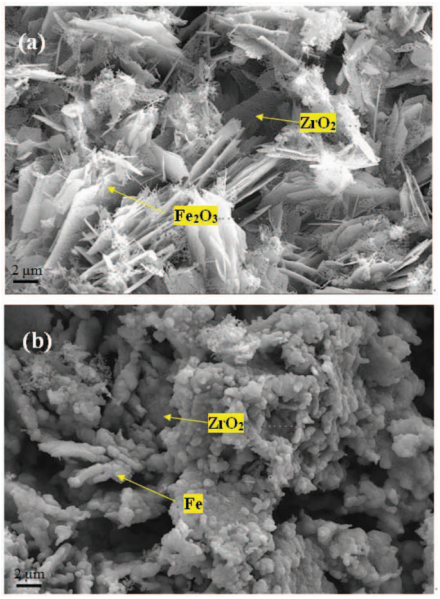

Figure 7. SEM images of active Fe nanoparticles inside Fe-based energy storage unit before (a) and after (b) tests.

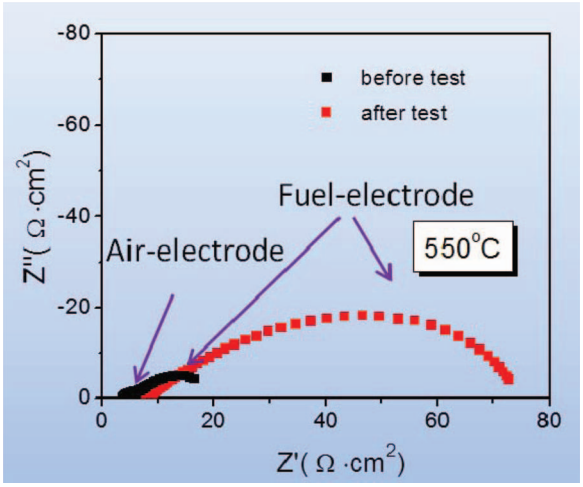

Figure 8. Comparison of AC impedance spectra measured from the baseline battery before and after cycling.

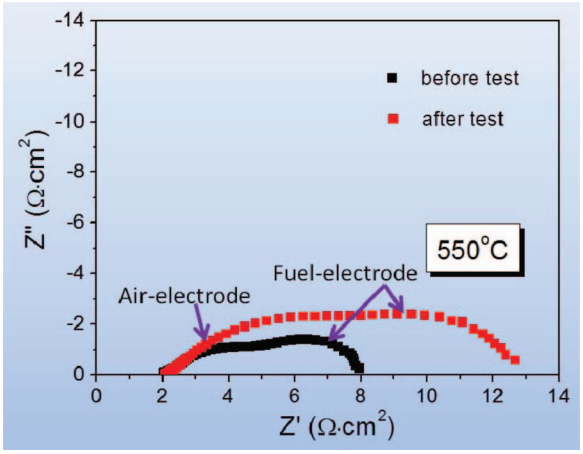

Figure 10. Comparison of AC impedance spectra before and after cycling measured from the optimized battery.

An ongoing effort to improve the overall performance of the battery.— We are currently working to improve the performance of RSOFC and redox kinetics of Fe-based energy storage. Fig. 9 shows the preliminary result of a most recently tested battery with thinner electrolyte, lower electrode resistance and better redox kinetics. To achieve the first two, a LSGM electrolyte membrane of 180 μm thick was screen-printed with a high- activity $Sm_{0.5}Sr_{0.5}CoO_{3-\delta}$-$Sm_{0.2}Ce_{0.8}O_{1.9}$ cathode[28] and a similar anode as the baseline battery. To further improve the anode performance, we also performed twice infiltrations of a $Ni(NO_3)_2$-$Gd(NO_3)_3$-$Ce(NO_3)_3$ solution (Ni:Gd:Ce = 0.70:0.24:0.06) into the anode structure. The results of Fig. 9 are very promising. Under the testing conditions of t = 550°C, J = 10 mA/cm^2 and cycle duration of 10 minutes, the newly developed battery yielded a DSE of 1,237 Wh/kg · Fe, which is up to 91.0% of MTSE, and a round trip efficiency of 82.5%, when compared with the CSE = 1,500 Wh/kg · Fe. The improved battery performance is a direct result of lowered ASRs of the RSOFC as is shown in Fig. 10. The initial ASR of the RSOFC is only 40% of the RSOFC used in the baseline battery. After cycling, the ASR increased only 5 Ω · cm^2, much less than 53 Ω · cm^2 observed in the post-tested RSOFC of the baseline battery. We will report more detail about this new development in the future.

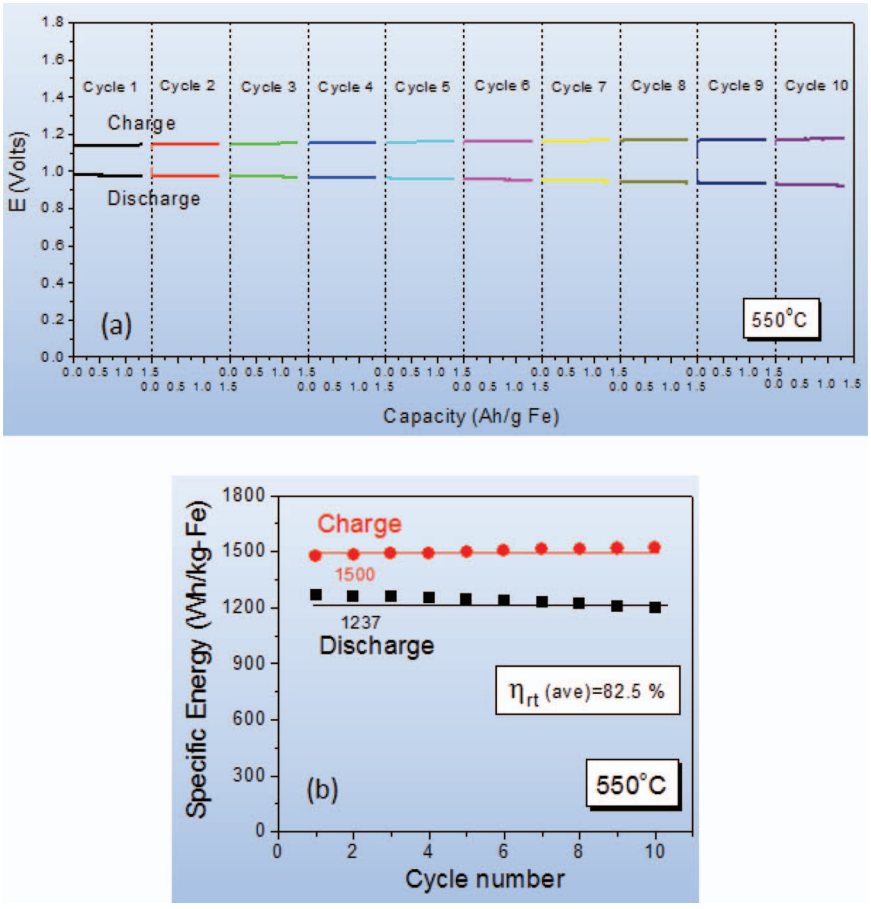

Figure 9. The performance of the optimized battery operated at 550°C for 10 continuous cycles with single-cycle duration of 10 minutes under a current density of 10 mA/cm^2 (a) E vs charge capacity; (b) averaged specific energy vs number of cycles.

Conclusions

The performance of three types of solid oxide "iron-air" batteries have been evaluated at 550°C in this study. The baseline battery comprised of Fe-Fe_3O_4 redox couple mixed with the ZrO_2 as a sintering inhibitor show a low discharge specific energy and round-trip efficiency. The second battery using the same Fe-Fe_3O_4 redox couple but infiltrated with CeO_2 nanoparticles exhibit a 15% and 29% improvement in discharge specific energy and round-trip efficiency over the baseline battery, respectively. The third battery using nanoparticle active Fe supported on a porous ZrO_2 substrate demonstrate 13% and 48% higher specific energy and round-trip efficiency, respectively, than the baseline battery. These improvements reflect the beneficial effects gained from enhanced catalytic activity offered by catalyst and increased reactive surface area derived from nanoparticles. An issue to the latter is the poor long-term cycle stability due to the coarsening of the nanoparticles under operating conditions.

Despite the improvements presented, the useable specific energy, round-trip efficiency and cycle stability of the battery remain to be further improved. An area that can lead to a significant advance in performance lies in the RSOFC. Thin-film electrolyte and high performance and stable electrode materials in RSOFCs is currently being tested in our laboratory with a goal to achieve higher specific energy, round-trip efficiency and better cycle stability. The preliminary results show that the discharge specific energy can reach 91.0% of the maximum theoretical specific energy with a round trip efficiency of 82.5%.

Acknowledgment

We thank University of South Carolina for supporting this work.

References

1. J. Lee, S. Kim, R. Cao, N. Choi, M. Liu, K. Lee, and J. Cho, *Adv. Ener. Mat.*, **1**, 34 (2011).
2. K. Harting, U. Kunz, and T. Turek, *Z. Phys. Chem. (Muenchen, Germany)*, **226**, 151 (2012).
3. B. L. Ellis, K. T. Lee, and L. F. Nazar, *Chem. Mater.*, **22**, 691 (2010).
4. S. R. Narayanan, G. K. Prakash, A. Manohar, B. Yang, S. Malkhandi, and A. Kindler, *Solid State Ionics*, **216**, 105 (2012).
5. Y. Shao, S. Park, J. Xiao, J.-G. Zhang, Y. Wang, and J. Liu, *ACS Catal.*, **2**, 844 (2012).
6. B. D. McCloskey, A. Speidel, R. Scheffler, D. C. Miller, V. Viswanathan, J. S. Hummelshøj, J. K. Nørskov, and A. C. Luntz, *J. Phy. Chem. Lett.*, **3**, 997 (2012).
7. H. Wang and K. Xie, *Electrochim. Acta*, **64**, 29 (2012).
8. Y. C. Lu, E. J. Crumlin, G. M. Veith, J. R. Harding, E. Mutoro, L. Baggetto, N. J. Dudney, Z. Liu, and Y. Shao-Horn, *Sci. Rep.*, **2**, 715 (2012).
9. S. A. Freunberger, Y. Chen, Z. Peng, J. M. Griffin, L. J. Hardwick, F. Bardé, P. Novák, and P. G. Bruce, *J. Am. Chem. Soc.*, **133**(20), 8040 (2011).
10. S. A. Freunberger, Y. Chen, N. E. Drewett, L. J. Hardwick, F. Bardé, and P. G. Bruce, *Angew. Chem. Intl. Ed.*, **50**(37), 8609 (2011).
11. N. Xu, X. Li, X. Zhao, J. B. Goodenough, and K. Huang, *Ener. & Environ. Sci.*, **4**(12), 4942 (2011).
12. X. Zhao, N. Xu, X. Li, Y. Gong, and K. Huang, *RSC Adv.*, **2**(27), 10163 (2012).
13. X. Zhao, N. Xu, X. Li, Y. Gong, and K. Huang, *ECS Trans.*, **45**, 113 (2013).
14. X. Zhao, N. Xu, X. Li, Y. Gong, and K. Huang, accepted, to be published in *ECS Trans.* (Volume 50), 2013.
15. X. Zhao, X. Li, Y. Gong, N. Xu, K. Romito, and K. Huang, *Chem. Commun.*, **49**, 5357 (2013).
16. J. W. Fergus, *J. Power Sources*, **162**, 30 (2006).
17. V. V. Kharton, F. M. B. Marques, and A. Atkinson, *Solid State Ionics*, **174**, 135 (2004).
18. S. P. S. Badwal and K. Foger, *Ceram. Intl.*, **22**, 257 (1996).
19. A. Inoishi, S. Ida, S. Uratani, T. Okano, and T. Ishihara, *Phys. Chem. Chem. Phys.*, **14**, 12818 (2012).
20. A. Inoishi, S. Ida, S. Uratani, T. Okano, and T. Ishihara, *RSC Advances*, **3**, 3024 (2013)
21. N. Xu, X. Li, X. Zhao, H. Zhao, and K. Huang, *Electrochemical and Solid-State Letters*, **15**(1), B1 (2012).
22. X. Li, N. Xu, X. Zhao, and K. Huang, *Journal of Power Sources*, **199**, 132 (2012).
23. X. Zhao, X. Li, N. Xu, and K. Huang, *Solid State Ionics*, **214**, 56 (2012).
24. K. Otsuka, T. Kaburagi, C. Yamada, and S. Takenaka, *Journal of Power Sources*, **122**, 111 (2003).
25. H. Kaneko, T. Miura, H. Ishihara, S. Taku, T. Yokoyama, H. Nakajima, and Y. Tamaura, *Energy*, **32**, 656 (2007).
26. K. Sohlberg, S. T. Pantelides, and S. J. Pennycook, *J. Am. Chem. Soc.*, **123**, 6609 (2001).
27. H. Kaneko, H. Ishihara, S. Taku, Y. Naganuma, N. Hasegawa, and Y. Tamaura, *J. Mater. Sci.*, **43**, 3153 (2008).
28. Z. Zhan, D. Han, T. Wu, X. Ye, S. Wang, T. Wen, S. Cho, and S. A. Barnett, *RSC Advances*, **2**, 4075 (2012).